

# Chemical characterization of size-selected nanoparticles emitted by a gasoline direct injection engine: impact of a catalytic stripper

Dumitru Duca<sup>a</sup>, Mostafiz Rahman<sup>b,1</sup>, Yvain Carpentier<sup>a</sup>, Claire Pirim<sup>a</sup>, Adam Boies<sup>b</sup>, Cristian Focsa<sup>a,\*</sup>

<sup>a</sup> *University of Lille, CNRS, UMR 8523 – PhLAM – Laboratoire de Physique des Lasers Atomes et Molécules, F-59000 Lille, France*

<sup>b</sup> *University of Cambridge, Department of Engineering, Cambridge, CB2 1PZ, United Kingdom*

---

## Abstract

This work combines laser desorption/ionization mass spectrometry (L2MS) and advanced statistical techniques to reveal the impact of a catalytic stripper (CS) on the chemical composition (at the molecular level) of a gasoline direct injection engine exhaust, and follow the evolution of size-dependent chemical characteristics over the whole particles size range (10–560 nm). The gas phase and polydisperse particles making up the exhaust are separated and sampled on distinct substrates using an original homebuilt two-filter system, while size-selected particles are collected using a cascade impactor and separated into 13 different size bins (smallest diameters 10–18 nm). We demonstrate that a fine molecular-level characterization of the exhaust particulate matter is necessary to assess the effect of the CS, especially for the smallest ultra-fine particles carrying the largest volatile fraction.

**Keywords:** Nanoparticles, Carbonaceous aerosols, Size-selective chemical characterization, Internal combustion engine, Catalytic stripper

---

---

<sup>\*</sup> *Corresponding author:* Cristian Focsa, University of Lille, CNRS, UMR 8523 – PhLAM – Laboratoire de Physique des Lasers Atomes et Molécules, F-59000 Lille, France  
*Phone:* +33 320 33 64 84, *Fax:* +33 320 33 64 63, *Email:* cristian.focsa@univ-lille.fr

<sup>1</sup> *Present address:* Institute for Future Transport and Cities, School of Mechanical Aerospace and Automotive Engineering, Coventry University, Coventry CV1 2JH, United Kingdom

## 1. Introduction

Internal combustion engine (ICE) powered vehicles constitute a major source of airborne particulate matter (PM), especially in urban areas [1, 2]. Particles emitted from vehicle engines are complex mixtures, mainly consisting of a carbonaceous core with a multitude of adsorbed compounds such as unburnt and partially oxygenated hydrocarbons, polycyclic aromatic hydrocarbons (PAHs), sulfates, and metal oxides [3, 4]. The particle's outer organic layer (the so-called surface organic fraction – SOF) exerts a considerable influence on the properties of particulate emissions (*i.e.* reactivity, toxicity, nucleation properties) and is considered a major contributor to particle-associated health hazards [5]. In this context, special attention is drawn by the ultra-fine particles (size  $<100$  nm) due to their higher deposition fraction, deeper penetration, and higher retention rate in the lungs [6, 7]. The inhalation of these smallest particles can result in health problems beyond the lungs: the presence of combustion derived nanoparticles has been detected in the frontal cortex of autopsy brain samples [8], urine of healthy children [9], and even in the fetal side of the placenta [10]. If transported to the fetus, these particles – as carriers for potentially toxic chemical species – could significantly affect fetal health and development [10]. Most recently, a strong association between increases in PM concentration and mortality rates due to COVID-19 was evidenced [11, 12].

The automotive industry has made significant efforts to reduce the amount and impact of internal combustion engine emissions [13–15]. For this purpose, various after-treatment systems based on conversion, adsorption and trapping technologies, such as three-way catalysts, diesel oxidation catalysts, selective catalytic reduction systems and particulate matter filters have been implemented in the exhaust track of both spark and compression ignition engines [16–18]. Devices providing chemical sites for oxidation and reduction reactions (*i.e.* catalytic strippers/converters) are particularly useful as they can convert toxic by-products present in the exhaust into less hazardous substances such as carbon dioxide, water vapor, and nitrogen gas. In the meantime, recent improvements in engine technology resulted in a significant decrease in the total number and mass of PM emitted by on-road vehicles. This, however, also led to a shift in the particle diameter toward smaller sizes (lower than 100 nm [19]).

34 Although not a major contributor to the emitted particle mass, these ultra-fine  
 35 sizes represent an important share in the total particle number (PN), which is  
 36 regulated by 17 out of the 20 countries of the G-20 group (accounting for 90%  
 37 of the global vehicle sales [20]). Current European Union (EU) regulations limit  
 38 PN emissions for sizes above 23 nm. However, sub-23nm particles are produced  
 39 in large concentrations by both Diesel and gasoline direct injection (GDI) en-  
 40 gines [21] and can sometimes reach 30–40% of the total PN for vehicles equipped  
 41 with a GDI [22]. Based on these findings, the PMP (particle measurement pro-  
 42 gramme) group of the working party on pollution and energy (GRPE) of the  
 43 United Nations Economic Commission for Europe (UNECE) has worked on a  
 44 protocol to lower the PM 23 nm cut-off point to 10 nm [23], the PM referring  
 45 only to solid (non-volatile) particles [24], *i.e.* those which do not evaporate below  
 46 350°C.

47 Lowering the cut-off size of measured PM might be quite challenging, as  
 48 it requires more efficient aerosol conditioning technologies to remove volatile  
 49 and semi-volatile compounds with minimal size-dependent particle losses and  
 50 to avoid the creation of artifacts (*i.e.* particles generated in the sampling /  
 51 conditioning system). Three EU Horizon 2020 projects [25–27] have worked in  
 52 parallel over the past few years to propose a robust methodology and associated  
 53 instrumentation (portable emissions measurement systems – PEMS) for PN  
 54 measurements down to 10 nm. Recent assessment campaigns [28–30] confirmed  
 55 that the developed PEMS prototypes are ready to be introduced in the future  
 56 regulations. A major change proposed in the PMP draft recommendations [23] is  
 57 to impose the use of a catalytic stripper (CS) as volatile particle remover (VPR)  
 58 in the future 10-nm PEMS, which is considered a safer option [31] than the  
 59 evaporation tube (ET) or the thermodenuder (TD). The ET, currently used in  
 60 automotive particle measurement systems, is a simple and robust method when  
 61 measuring particles larger than 23 nm as it is able to completely evaporate most  
 62 hydrocarbons. However, this technology might lead to re-nucleation of semi-  
 63 volatile species at high hydrocarbon particle concentrations and thus higher  
 64 primary dilution ratios are required to reliably measure solid particles smaller  
 65 than 23 nm [32, 33]. Therefore, for measuring particles in the sub-23 nm range,  
 66 removing the semi-volatile aerosol fraction using a CS optimized for small losses

67 of ultra-fine particles can prove more efficient [34–36].

68 The use of CSs in emission measurement systems has been reviewed by  
69 Giechaskiel et al. [31]. Up to now, the impact of CSs on the resulting emissions  
70 has mostly been characterized physically, with comparisons between stripped  
71 and unstripped particle mass, number or size distribution. What comes into  
72 view is the current lack of information regarding its impact on the chemical  
73 composition (at the molecular level) of the emitted aerosols (with the notable  
74 exception of one study addressing marine exhaust aerosols [37]). As the chemical  
75 composition (and thus the degree of volatility) making up the SOF layer can  
76 significantly vary with engine regimes or with PM size, an extensive investigation  
77 of the physico-chemical properties of the measured objects should be undertaken  
78 to ensure the development of a PEMS instrument capable of maintaining its  
79 accuracy and reliability for a wide range of engine operating conditions (*i.e.* in  
80 real driving conditions).

81 In the frame of the EU Horizon 2020 PEMS4Nano project [25] we conducted  
82 extensive measurement campaigns to thoroughly analyze the physico-chemical  
83 properties of particles emitted by a single-cylinder engine in a bottom-up ap-  
84 proach combining experimental [38] and theoretical studies [39] for the devel-  
85 opment of a PEMS prototype. The action of a home-made (University of Cam-  
86 bridge) CS on the measured aerosol (polydisperse and size-selected particles,  
87 gas phase) was investigated both on-line (physical characterization by an origi-  
88 nal tandem arrangement of aerodynamic aerosol classifier, differential mobility  
89 analyzer, and centrifugal particle mass analyzer [40]) and off-line (laser mass  
90 spectrometry chemical characterization of filter-collected samples). As on-line  
91 chemical characterization by aerosol mass spectrometers is limited to particles  
92 larger than  $\sim 50\text{nm}$  [37], the off-line approach adopted here is the only possible  
93 solution when focusing on smaller nanoparticles (10–32 nm in the present study)  
94 of actual interest for the 10-nm PEMS development.

## 95 **2. Materials and methods**

### 96 *2.1. Sampling*

97 A generic single-cylinder gasoline direct injection engine was used on a test  
98 bench to generate particles with various properties for building an extensive

99 database through multi-technique physico-chemical characterization [38]. The  
 100 engine was described in detail in a previous publication [38], only the main  
 101 characteristics are briefly reminded in Table 1, Supporting Information. For  
 102 the present study, two set-points were used, called in the following low speed  
 103 (LS, 1200 rpm) and high speed (HS, 2000 rpm). The IMEP (indicated mean  
 104 effective pressure) was kept constant at 10 bar,  $\lambda$  at 1.01, and the injection  
 105 at 270° bTDC (before top-dead center). The engine was operating on Euro  
 106 Stage V E5 Gasoline (CEC-RF-02-08 E5) with the ignition timing set for the  
 107 maximum brake torque (MBT). The temperature of both coolant and oil (Agip  
 108 SIGMA, 10W-40) was kept at 80°C. To ensure the cleanliness of the combustion  
 109 chamber, the engine was conditioned with methane (CH<sub>4</sub>) before changing the  
 110 operating point.

Table 1: Engine specifications (b/aTDC – before/after Top Dead Center)

Specification		Value
Cylinder head		Pentroof type
Compression ratio		12.5:1
Bore		82 mm
Stroke		85 mm
Displacement		449 cm <sup>3</sup>
Fuel direct injection system		Central mounted generic six-hole injector
Injection pressure		150 bars
Spark plug location		Exhaust side
Intake valve timing:	Open	334 deg. bTDC
	Close	166 deg. bTDC
Exhaust valve timing:	Open	154 deg. aTDC
	Close	330 deg. aTDC

111 A custom sampling line (Figure 1) was used for the simultaneous collection  
 112 of engine exhaust for offline characterization and online volatile mass fraction  
 113 measurements [40]. Raw engine exhaust was sampled from the exhaust pipe 10  
 114 cm downstream of the manifold. Sampled flow was then diluted using a Dekati  
 115 FPS 4000 (1:30 dilution ratio) to prevent the condensation of volatile species as  
 116 well as their aggregation. The main objective of this study was to assess the im-  
 117 pact of the catalytic stripping on the gas phase, polydisperse, and size-selected  
 118 particles. Two CSs were used: CS1 (1.5 l/min flow) for on-line measurements  
 119 (Catalytic Instruments CS-015) and CS2 (presented in detail in reference [38]),

120 which was manufactured identical to CS1 by the University of Cambridge with  
 121 the exception that it was adapted to accept higher flows (10 l/min) to increase  
 122 the exhaust collection efficiency needed for the subsequent offline analysis. Both  
 123 CSs performances in terms of hydrocarbon removal were tested to be >99% for  
 124 30 nm tetracontane ( $C_{40}H_{82}$ ) particles at a concentration of  $>10^4 \text{ cm}^{-3}$ . As this  
 125 work focuses on the offline analysis, only the corresponding experimental details  
 126 are given below, while information about the online measurement can be found  
 127 in reference [40]. The upstream (unstripped) flows were analyzed/sampled us-  
 128 ing bypasses (red dashed lines in Figure 1), while the downstream (stripped)  
 129 flows were collected after passing through the CS. The sampling of size-selected  
 130 particles was performed with a NanoMOUDI II cascade impactor (TSI, model  
 131 125R) able to separate particles into 13 different size-bins, with nominal cut  
 132 sizes of 10000, 5600, 3200, 1800, 1000, 560, 320, 180, 100, 56, 32, 18, 10 nm.  
 133 The size-selected particles were deposited on aluminum foils that were cleaned  
 134 and thermally treated (at  $300^\circ\text{C}$ ) prior to the sampling to remove all possible  
 135 surface contaminants. The sampling time varied between 6h and 12h. An alter-  
 136 native (separate) sampling of polydisperse particles and exhaust gas phase was  
 137 performed with an original double-filter system recently developed in our labora-  
 138 tory [41]. This device is made of two quartz fiber filters (QFF) placed in series:  
 139 the front filter (FF) retains the particulate matter while letting through the  
 140 gas/volatile phase, which is then adsorbed by a layer of activated carbon placed  
 141 on the back filter (BF). This sampling system was proven to be very efficient  
 142 in separating the particulate (non-volatile) and the gas phases in combustion  
 143 emissions [41]. Both front and back filters were thermally conditioned before  
 144 the sampling in order to remove any possible contaminants. The sampling time  
 145 was adjusted (60–80 min) in accordance with the particle concentration and size  
 146 distribution in the exhaust to obtain a homogeneous layer of particles on the  
 147 FF.

148 A total of 44 samples were collected in the two engine regimes for subsequent  
 149 offline analysis. A sample labeling scheme is used in the following, indicating the  
 150 engine set-point (HS or LS), the downstream (CS) or upstream sampling point,  
 151 the size-bin (for size-selected particles) or the collection QFF in the double-  
 152 filter device (FF for polydisperse particles, BF for gas phase). For instance,

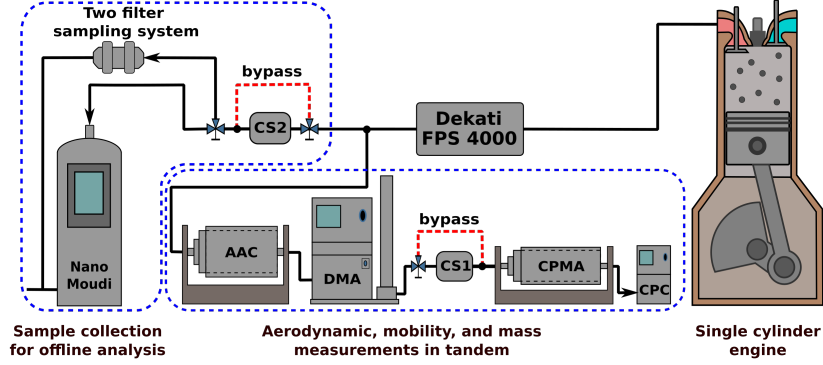


Figure 1: Schematic representation of the experimental setup. Sampling of the exhaust was conducted with a NanoMoudi II cascade impactor to size-select particles and a two-filter collection device [41] to separate the PM (polydisperse particles) and the gas phase. The collection was performed with and without the CS. The online SOF mass fraction measurements were performed with a combination of Aerodynamic Aerosol Classifier (AAC, Cambustion Ltd.), differential mobility analyzer (3080 DMA, TSI Inc.), and centrifugal particle mass analyzer (CPMA, Cambustion Ltd.) followed by a condensation particle counter (CPC, 3776, TSI Inc.) [40].

153 HS-CS<sub>FF</sub> indicates polydisperse particles collected downstream the CS in HS  
 154 engine regime, while LS<sub>10–18</sub> labels 10–18 nm size-selected particles collected  
 155 upstream the CS in the LS engine regime. In addition, a set of blank samples  
 156 (aluminum foil, a neat QFF, and an activated carbon-covered QFF) were pre-  
 157 pared, stored (at 4°C) and managed in a similar way than the collected samples.

## 158 2.2. Chemical analysis

159 The chemical characterization of collected particles was performed using a  
 160 two-step (desorption/ionization) laser mass spectrometry technique (L2MS) de-  
 161 scribed in detail elsewhere [42, 43]. The mass spectrometer used in this study  
 162 (Fasmatech S&T) combines ion cooling, Radio Frequency (RF) guiding and  
 163 Time-of-Flight (ToF) analyzer to reach a mass resolution of  $\sim 15000$ . The sam-  
 164 ple, placed under vacuum ( $10^{-8}$  mbar residual pressure), is irradiated at  $30^\circ$  an-  
 165 gle of incidence by a frequency doubled Nd:YAG laser beam (Quantel Brilliant,  
 166  $\lambda_d = 532$  nm, 4 ns pulse duration,  $0.10\text{--}0.22$  J cm $^{-2}$  fluence, 10 Hz repetition rate)  
 167 focused to a  $0.07$  mm $^2$  spot on the surface. The desorbed compounds form a  
 168 gas plume that expands in the vacuum normally to the sample surface, and are  
 169 ionized by an orthogonal UV laser beam (Quantel Brilliant,  $\lambda_i = 266$  nm, 4 ns

170 pulse duration, 10 Hz repetition rate,  $\sim 0.3 \text{ J cm}^{-2}$  fluence). The generated ions  
 171 are then RF-guided to a He collision cell for thermalization and subsequently  
 172 mass analyzed in a time-of-flight mass spectrometer equipped with a reflectron  
 173 (ToF-MS). The desorption and ionization fluences were adjusted for each sample  
 174 to obtain the maximum signal intensity while minimizing fragmentation in the  
 175 mass spectra. Each mass spectrum was obtained by averaging the signal from  
 176 200 laser shots applied on a small ( $\sim 2 \text{ mm}^2$ ) zone of the sample. To check the  
 177 homogeneity of the sample surface, the analysis was performed on four different  
 178 zones of each sample and all the results were used in the subsequent statistical  
 179 data treatment.

180 Since mass spectra of the analyzed samples contain a large number of peaks  
 181 its interpretation can be challenging. To optimally exploit this large amount of  
 182 information, the MS data treatment follows a dedicated methodology developed  
 183 in our group [44–46], which includes mass defect and multivariate analysis ap-  
 184 proaches. In this framework, a variety of advanced statistical techniques such as  
 185 Principal Component Analysis (PCA) [47], Hierarchical Clustering on Principal  
 186 Components (HCPC), and volcano plots [48, 49] can help uncover “hidden” pat-  
 187 terns in complex datasets, group samples based on their similarities and identify  
 188 the most significant mass peaks contributing to sample differentiation.

### 189 **3. Results and discussion**

#### 190 *3.1. Polydisperse particles and gas phase*

191 The impact of the catalytic stripper on polydisperse PM and the gas phase  
 192 was assessed by comparing the chemical composition of samples collected with  
 193 and without the CS. Examples of mass spectra recorded for polydisperse parti-  
 194 cles (FF) and gas phase (BF) samples collected (in the high-speed engine regime)  
 195 upstream and downstream the CS are displayed in Figure 2. The spectra contain  
 196 predominantly polycyclic aromatic species and their fragments; their partial ion  
 197 count (PIC) was shown to be representative of the organic carbon content of the  
 198 sample [38, 46, 50]. When comparing downstream (HS-CS<sub>FF</sub>) and upstream  
 199 (HS<sub>FF</sub>) particles, a 7-fold reduction of aromatic PIC is observed, which clearly  
 200 demonstrates the efficiency of the CS in stripping the surface organic layer. Al-  
 201 though a direct quantitative comparison is not possible (different experimental

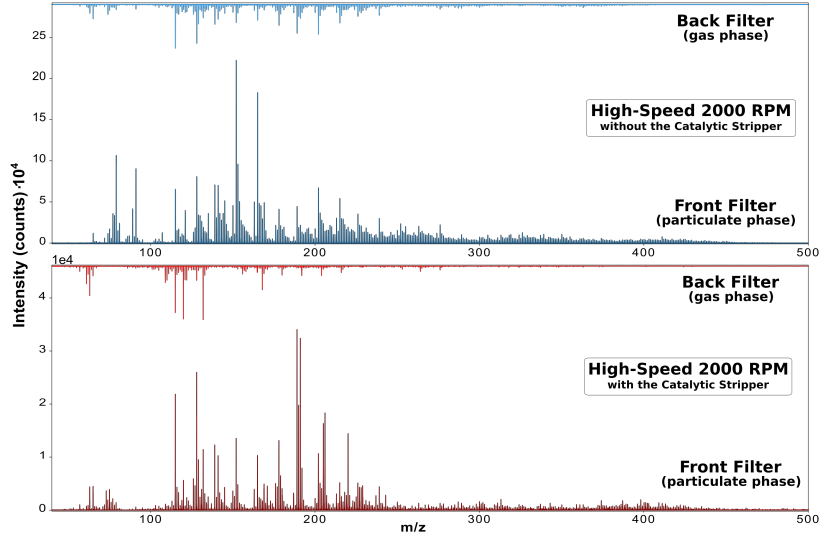


Figure 2: Mass spectra of  $\text{HS}_{FF/BF}$  and  $\text{HS-CS}_{FF/BF}$  samples (particulate and gas phase collected with and without the CS) obtained with L2MS.

configurations), we note that this efficiency is in line with previous measurements performed with a soot particle aerosol mass spectrometer (SP-AMS) on marine engine exhaust, where organic species reductions in the range 94-97% were observed upon stripping [37]. The relatively small difference between the results presented here and the ones reported in Amanatidis et al. [37] might be explained by the fact that the SP-AMS instrument is only able to measure particles larger than  $\sim 50$  nm and the smallest particles below this threshold are expected to carry a higher SOF. A detailed discussion on this will be provided in the section 3.2, which focuses on size-selected particles (especially the 10–32 nm range). The efficiency of the CS in removing organics is even higher on the gas phase, as a 20-fold reduction in aromatic PIC was recorded downstream ( $\text{HS-CS}_{BF}$  sample) with respect to upstream ( $\text{HS}_{BF}$ ). Indeed, the mass spectrum of the  $\text{HS-CS}_{BF}$  sample contains mostly carbon clusters ( $\text{C}_n^+$ , representative of the elemental carbon content [38, 46]) and is almost identical to the blank BF spectrum. We emphasize that the presence of carbon clusters on back filters, sampled both with and without the CS, is determined by the layer of activated carbon intended to trap the gas phase [41] and cannot be associated with the exhaust gas phase combustion by-products.

To properly interpret mass spectrometric data, mass defect analysis [44–46]

221 was used to assign chemical formulas to the most intense peaks. The full list  
 222 of assigned peaks is provided in Table S1. A volcano plot [48, 49] was used to  
 223 highlight the CS-induced changes in the chemical composition of both particu-  
 224 late and gas phases. The two phases carry chemical species of different volatility  
 225 and mass, and thus the separate study of these phases allows to better evaluate  
 226 the efficiency of the CS. The differences between the chemical composition of  
 227 the particulate and gas phases can clearly be seen when the front (particulate  
 228 phase) and the back filter (gas phase) sampled without the CS are compared,  
 229 Figure S1. The front filter receives a high contribution from higher-mass aro-  
 230 matic species, with more than 4 aromatic rings. According to Bari et al. [51],  
 231 the volatility of aromatic compounds can be inferred from the total number of  
 232 aromatic rings: compounds consisting of only two aromatic rings are considered  
 233 volatile, three to four – semi-volatile, and those with more than four aromatic  
 234 rings – non-volatile. It should be noted that all the peaks corresponding to car-  
 235 bon clusters ( $C_n^+$ ) have been excluded from this analysis since, in this case, they  
 236 do not originate from the same source (soot particles for the front filters and the  
 237 pre-applied black carbon layer for the back filter). However, when comparing  
 238 only front filter samples (Figure 3a), carbon clusters provide important infor-  
 239 mation about the variation of the OC/EC ratio (organic carbon to elemental  
 240 carbon content) of sampled particles as they are commonly considered as mark-  
 241 ers of EC [46, 52–54]. Once the particles pass through the CS the contribution of  
 242 aromatic compounds, considered as good indicators of the organic carbon con-  
 243 tent [38, 50], is significantly reduced, effectively decreasing the OC/EC ratio.  
 244 Moreover, stripped particles feature a higher contribution from oxygenated and  
 245 nitrogenated species which can be linked to the oxidation processes occurring  
 246 in the CS.

247 A similar picture can be seen when the two samples corresponding to the  
 248 gas phase ( $HS_{BF}$  and  $HS_{CS_{BF}}$ ) are compared, Figure 3b. The gas phase  
 249 sampled without the CS presents a high content of aromatic compounds (mostly  
 250 low-mass, up to 4 aromatic rings), while the one collected downstream the  
 251 stripper is characterized only by carbon clusters (coming from the underlying  
 252 black carbon layer). The fact that no organic species contribute in a significant  
 253 way to the  $HS_{CS_{BF}}$  mass spectrum implies that the CS removed the majority

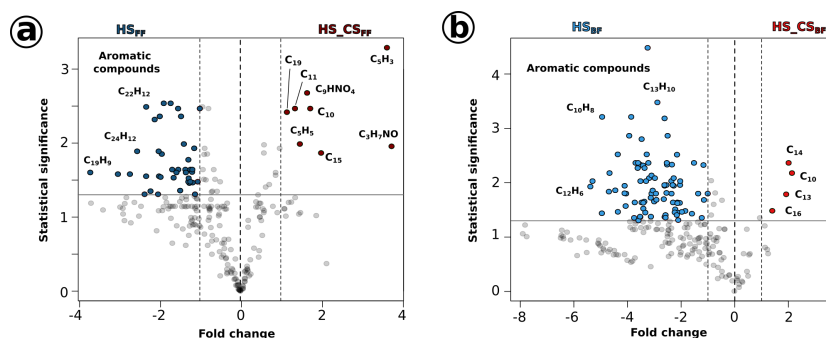


Figure 3: Volcano plots showing the “differential expression” of detected chemical species: a) comparison between the chemical composition of the particulate phase sampled with and without the CS, and b) influence of the CS on the chemical composition of the gas phase.

of combustion-generated compounds from the gas phase.

A principal component analysis of all FF and BF samples collected (with and without the CS) in both engine regimes (HS and LS) was performed. This approach allows the differentiation between samples and highlights (through the analysis of the loading plots, Figure S2) the contribution of individual compounds or groups of highly correlated species to this differentiation. The PCA was able to separate all the samples with only two principal components accounting for  $\sim 72\%$  of the total variance. The first principal component ( $\sim 63.9\%$ ) separates the samples based on the OC/EC ratio (a high positive PC1 score reflects a low OC/EC ratio). The volatility of the samples can be inferred from their PC2 ( $\sim 8.2\%$  of explained variance) scores. A positive PC2 score is associated with the presence of non-volatile aromatic species (more than 4 aromatic rings) with  $m/z \leq 363$ , while a negative PC2 score is linked to the presence of volatile and semi-volatile compounds, as well as some high-mass aromatic species ( $m/z > 363$ ). Three major regions can be seen on the score plot presented in Figure 4: i) particulate phase sampled without the CS ( $HS_{FF}$  and  $LS_{FF}$ , dark blue), ii) particulate phase sampled with the CS along with the gas phase sampled without it ( $HS_{CS_{FF}}$ ,  $LS_{CS_{FF}}$  – dark red,  $HS_{BF}$ , and  $LS_{BF}$  – light blue), and iii) the gas phase collected after the CS ( $HS_{CS_{BF}}$  and  $LS_{CS_{BF}}$  - light red).

It is worth noting that even though particulate phases sampled without the stripper are located fairly close to each other and can be grouped together, their chemical composition is different. The PC1 score for the front filter (par-

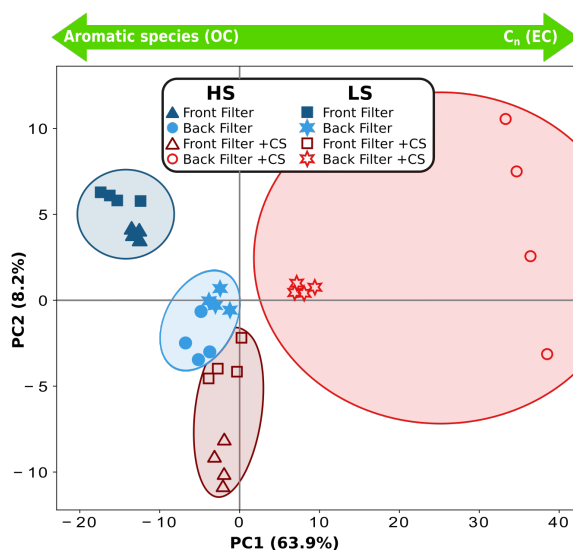


Figure 4: Score plot of the first two principal components for the particulate and gas phase samples collected with and without the CS in two different engine regimes (HS and LS). The arrows represent the meaning of the first principal component derived from the corresponding loadings plot, Figure S2.

276 ticulate phase) collected in the LS engine regime is lower, thus indicating a  
 277 higher contribution from organic compounds in this regime. However, after the  
 278 catalytic treatment, particles emitted in different engine regimes seem to have  
 279 a more similar chemical composition, depicted by their almost identical PC1  
 280 scores. Moreover, the sign of the PC2 value changes after the particles have  
 281 passed through the CS, suggesting the removal of the vast majority of high-  
 282 mass organic compounds. The untreated gas phase contains a much smaller  
 283 amount of organic species (PC1 value close to zero) which are almost com-  
 284 pletely removed by the stripper (PC1 sign changes). Therefore, mass spectra  
 285 of HS-CS<sub>BF</sub> and LS-CS<sub>BF</sub> samples have a much larger contribution from the  
 286 layer of activated carbon pre-applied to their surfaces, and thus the difference  
 287 in PC1 value (*i.e.* contribution of elemental carbon) between the two samples  
 288 cannot be attributed to combustion conditions and instead is determined by  
 289 small inhomogeneities in the layer of activated carbon. The PC2 value for gas  
 290 phase samples is close to zero, indicating a low influence from this component  
 291 due to the insignificant number of high-mass organic species.

292 A volcano plot (Figure S3) was employed to compare the particulate phase

293 produced in the HS and LS engine regimes. When comparing unstripped par-  
 294 ticles, Figure S3a, we can see that while both samples contain a large amount  
 295 of aromatic compounds, the one obtained at lower speed (LS) contains more  
 296 high-mass species (*i.e.* non-volatile compounds [41, 51]). Unstripped parti-  
 297 cles collected in different regimes have a noteworthy difference in the chemical  
 298 composition, demonstrated by the fact that 55 compounds contribute in a sta-  
 299 tistically significant way to their separation. In contrast, stripped particles  
 300 appear to be very similar, Figure S3b. Only a few species contribute to the  
 301 separation between the mass spectra of stripped particles generated in different  
 302 engine regimes, and these mass spectra are mostly constituted of carbon clus-  
 303 ters (representative of EC). This is an important result, showing that the CS  
 304 is able to treat particles exhibiting quite different initial chemical composition,  
 305 effectively stripping their (different) surface organic layers and leaving them as  
 306 solid non-volatile PM.

### 307 *3.2. Size-selected particles*

308 Size-selected particles produced in the two engine regimes, and sampled with  
 309 or without the CS were chemically characterized. For the first engine regime  
 310 (HS) the stages of the cascade impactor that collected sufficient material (with  
 311 and without the CS) covered a quite extended size-range: from 10 nm up to  
 312 560 nm (HS<sub>10–18</sub> – HS<sub>320–560</sub> samples). Mass spectra of these samples are  
 313 presented in Figure 5. One can see that mass spectra of particles from different  
 314 size-bins are very different, indicating that the chemical composition of emitted  
 315 particles significantly changes with the size. Mass spectra of particles collected  
 316 without the CS show a high contribution from heavy-mass PAHs that can be  
 317 associated with the remnants of the fuel or lubricating oil [38]. The majority  
 318 of these compounds are successfully removed by the CS, which is illustrated by  
 319 the decrease in the absolute signal intensity. At the same time the contribution  
 320 of carbon clusters ( $C_n^+$ ) increases, thus indicating a much lower OC/EC ratio  
 321 for the stripped particles. The relative contribution of low-mass PAHs and their  
 322 fragments increases toward smaller particle sizes which suggests an increase in  
 323 the overall volatility of the surface organic fraction [40].

324 PCA was applied to the mass spectrometric data to study the impact of CS  
 325 on the size dependent chemical composition. The first two principal components

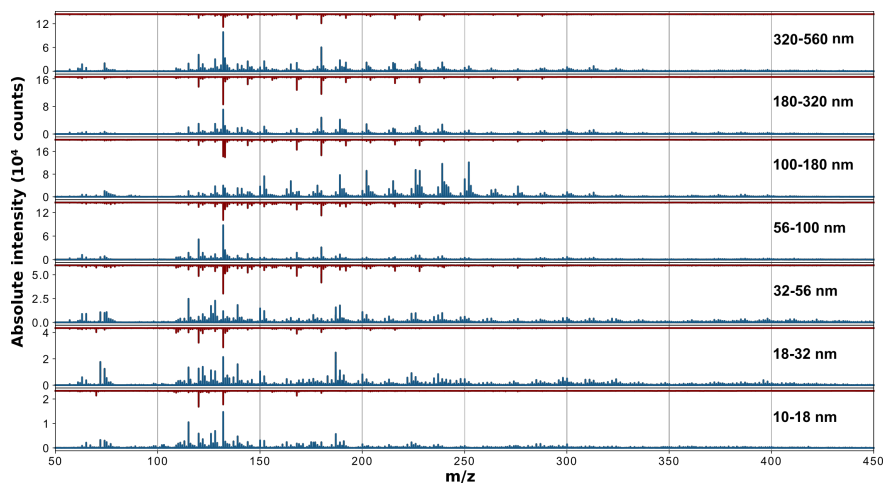


Figure 5: Mass spectra of size-selected particles produced in the HS engine regime and sampled with (red line – HS\_CS) and without (blue line – HS) the catalytic stripper. The labels indicate the corresponding NanoMOUDI size-bin.

326 account for  $\sim 60\%$  of the variance in the dataset and are able to discriminate  
 327 between different samples (with particles of a different size and collected with or  
 328 without the catalytic stripper), Figure 6a. The meaning of each component was  
 329 determined from its corresponding loadings plot, Figure S4. The first principal  
 330 component (PC1) separates samples based on the contribution to mass spectra  
 331 of aromatic species (OC – positive PC1 scores) and carbon clusters ( $C_n^+$ , EC  
 332 – negative PC1 scores). Therefore, this component enables the discrimination  
 333 between particles with a different OC/EC ratio. The HS samples have mainly  
 334 positive PC1 scores while HS\_CS ones – mostly negative, thus indicating that  
 335 a significant amount of the organic fraction was removed from the particles  
 336 by the CS. It is worth noting that the smallest analyzed particles (10–32 nm,  
 337 HS<sub>10–18</sub> and HS<sub>18–32</sub>) are the most affected by this treatment (revealed by the  
 338 large separation between HS<sub>10–18,18–32</sub> and HS\_CS<sub>10–18,18–32</sub> data points in  
 339 the score plot, Figure 6a). This separation can be associated with the high  
 340 relative content of organic species present on smaller particles which is almost  
 341 completely removed by the CS and leading to a significant change in the PC1  
 342 score (OC/EC). Once the organic fraction is removed, the signal related to the  
 343 elemental carbon (EC) becomes more important ( $C_n^+$  ions), leading to a negative  
 344 PC1 score.

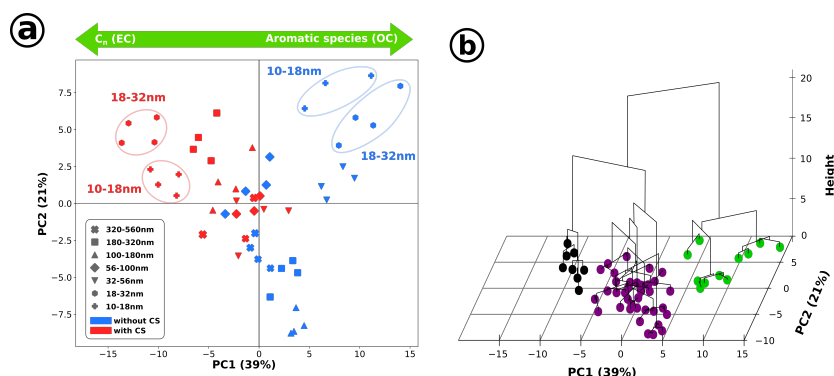


Figure 6: Impact of the CS on size-dependent PM chemical composition: a) Score plot of the first two principal components obtained from mass spectra of size-selected particles collected with (red symbols) and without (blue symbols) the CS in the HS engine regime; the arrows show the meaning of the principal components obtained from their loadings, and b) HCPC performed on the first five principal components (explaining more than 82% of the variance); three biggest clusters correspond to: small particles collected with the CS (HS\_CS<sub>10–18</sub> and HS\_CS<sub>18–32</sub>) – black markers, small particles collected without the CS (HS<sub>10–18</sub>, HS<sub>18–32</sub>, and HS<sub>32–56</sub>) – green markers, and bigger particles collected in both regimes (HS and LS) – purple markers.

345 The second principal component is related to the presence of PAHs (*i.e.*  
 346 stabilomers [55], negative PC2 score). Smaller particles (<100 nm) show a  
 347 high contribution from fragments and PAH derivatives (positive PC2) while  
 348 bigger particles (100–560 nm) contain a larger number of stabilomer PAHs that  
 349 are removed by the CS (PC2 score changes from being negative to positive or  
 350 almost zero). It should be noted that the spread between data points across  
 351 the second dimension (PC2) is much smaller for particles collected with the CS  
 352 (HS\_CS), indicating that, when it comes to the organic fraction, the chemical  
 353 composition of stripped size-selected particles is not very different.

354 HCPC was performed on the first five principal components, accounting for  
 355 more than 82% of the variance within the data set, to identify the clusters  
 356 that form in the principal component space and discriminate between particles,  
 357 Figure 6b. Three separate clusters can be identified: small particles collected  
 358 with the CS (HS\_CS<sub>10–18</sub> and HS\_CS<sub>18–32</sub>) – black markers, small particles col-  
 359 lected without the CS (HS<sub>10–18</sub>, HS<sub>18–32</sub>, and HS<sub>32–56</sub>) – green markers, and  
 360 bigger particles collected in both regimes – red markers. This shows that the  
 361 chemical composition of the smallest particles was significantly changed by the

362 CS, thus supporting our previous conclusion that small particles contain a high  
363 surface organic fraction which makes them more susceptible to a catalytic treat-  
364 ment. This conclusion is also supported by online aerodynamic-mass-mobility  
365 measurements that show that the volatile mass fraction increases for smaller  
366 particles, Figure S8.

367 The compounds that are efficiently removed from the smallest particles (10–  
368 18 nm) by the stripper were identified with a volcano plot, Figure S5. The  
369 CS removes the organic fraction from these particles, leading to the decrease  
370 of the OC/EC ratio. It is worth noting that, for this particular size-bin, the  
371 CS effectively removes PAHs from the entire mass-range and particles end up  
372 showing only a negligible contribution from organic species.

373 As the chemical composition of the emitted particles depends on the engine  
374 set-point, the CS may impact differently particles belonging to the same size-bin  
375 but generated in different engine regimes (LS or HS). To identify the (possible)  
376 change in CS efficiency, the differences between the initial (unstripped) chemical  
377 compositions of size-selected particles produced in the two engine regimes must  
378 be first identified with PCA (Figure 7a). The first two principal components  
379 account for 61% of the variation in the data set and will be used to explain the  
380 differences in the chemical composition. From the loadings plot (Figure S6a),  
381 PC1 can be linked to the contribution of PAHs (positive value), fragments, and  
382 carbon clusters (negative PC1), while PC2 can be used to separate samples  
383 based on the OC/EC ratio. For instance, samples with a low OC/EC ratio have  
384 a negative PC2 score, while the ones with a high amount of organic species  
385 exhibit a positive PC2 value. On the score plot (Figure 7a) the data points  
386 corresponding to the two engine regimes are well separated by PC1. Therefore,  
387 it is possible to distinguish between particles produced in these two regimes  
388 based only on the contribution of PAHs, fragments, and carbon clusters. PM  
389 collected in the LS engine regime features a much higher contribution from  
390 PAHs, with particles from all size-bins having a negative PC1 score (except for  
391 LS<sub>10–18</sub>). In contrast, particles emitted in the HS engine regime exhibit a higher  
392 signal coming from fragments and carbon clusters. Note that the fact that HS  
393 samples show a positive PC1 score cannot be linked to a missing organic fraction  
394 and should only be seen as a lower relative contribution of the peaks attributed

to organic species compared to that observed for LS samples. PC2 shows that in the LS regime, the smallest particles yield the highest OC/EC ratio, also higher than that of the corresponding HS sample. The biggest particles (56–560 nm) produced in the HS regime show the highest contribution from carbon clusters, *i.e.* the lowest OC/EC. In addition, smaller particles from the HS regime (10–100 nm) show the highest partition of organic species. Particles in the size range of 100–320 nm produced in both regimes display a similar PC2 score, implying that they are the least affected by the change in engine operating conditions.

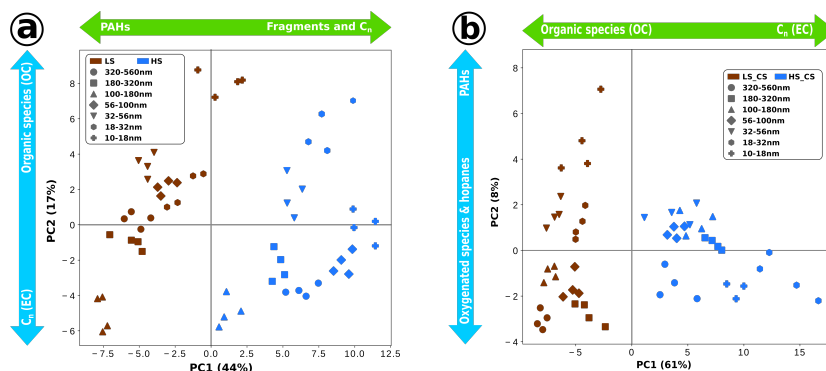


Figure 7: Score plot of the first two principal components obtained from the mass spectra of size-selected particles collected in the LS and HS engine regimes without (a) and with (b) the catalytic stripper. The arrows indicate the meaning of principal components obtained from their corresponding loadings.

Once the differences between the chemical compositions of unstripped particles produced in the two engine regimes have been identified, the effect of the CS on size-selected PM with different chemical composition can be determined by PCA, as shown in Figure 7b. The first two principal components explain 69% of the observed variance and are able to distinguish between stripped particles generated in the two engine regimes based on the few chemical species left on the surface. The first principal component (61%) groups samples based on their OC/EC ratio, determined from the corresponding loadings plot (Figure S6b). It should be noted that PCA is emphasizing the variance in the dataset, and thus the separation between particles observed on the score plot (Figure 7b) cannot be used to quantify, for instance, the difference in the organic content. The majority of organic species present on raw particles are successfully stripped by the CS, making their chemical composition comparable, similar to what was shown

before for polydisperse particles. However, the high sensitivity of the analytical technique [43] used here reveals distinct features in size-selected stripped particles collected in different engine regimes. For instance, when comparing the smallest treated particles (10–18 nm) collected in different engine regimes with a volcano plot (Figure S7) we can see that only a few species contribute to the separation between the samples. Due to their small mass, the chemical information related to these particles is usually lost when polydisperse PM is collected, thus illustrating the importance of size-selective analysis. The spread between data points on the PC1 axis is rather small, suggesting that stripped particles of different sizes have a comparable amount of OC.

The second principal component is linked to the amount of aromatic species (positive PC2 score), oxygenated, and hopanoid compounds (negative PC2 score). The latter group of compounds is often used as marker species for remnants of lubricating oil [38]. The CS successfully removes these compounds from particles smaller than 100 nm, however, bigger LS\_CS particles (100–560 nm) still contain residues of these compounds. Even though particles in three size-bins sampled in the HS\_CS engine regime (HS\_CS<sub>320–560</sub>, HS\_CS<sub>18–32</sub>, HS\_CS<sub>10–18</sub>) also show a negative PC2 score, they do not exhibit a high hopanoid content but are instead characterized by a higher content of oxygenated species (identified from volcano plots). The HS\_CS cluster is located very close to the PC2 axis, suggesting, once again, their lower OC/EC ratio compared to LS\_CS particles.

#### 4. Conclusions

To the best of our knowledge, this is the first study to tackle a detailed, molecular-level characterization of the impact of a CS (in a PEMS context) on the chemical composition of an ICE exhaust. Most of the studies test the CS removal efficiency on tetracontane (C<sub>40</sub>H<sub>82</sub>) particles, following the recommendations of the PMP protocol [20]. Amanatidis et al. [35] used liquid decane (C<sub>10</sub>H<sub>22</sub>) and toluene (C<sub>7</sub>H<sub>8</sub>) injected in a 10% v/v O<sub>2</sub> in N<sub>2</sub> gas mixture to measure efficiencies >90% for the removal of these hydrocarbons by a CS, while preliminary tests with a heavier (C<sub>16</sub>) species led to artifacts and inconclusive results. In another study, Amanatidis et al. [37] measured stripping efficiencies

448 of organics in the range 94-97% from particles ( $>50$  nm) emitted by a marine  
449 engine. The results of the present study on polydisperse particles and gas phase  
450 emitted by a single-cylinder GDI are well in line with those previous findings  
451 and foster the use of a CS-based VPR system in future PEMS.

452 A specificity of our work is the study of the chemical composition of particles  
453 selected by size. Indeed, the composition of engine exhaust PM can significantly  
454 change not only with the engine set-point but also with the particle size [38].  
455 When polydisperse PM is studied, a weighted average composition of particles  
456 of various sizes is obtained, with individual weights related to the initial par-  
457 ticle size distribution which can significantly change depending on the engine  
458 set-point. This is clearly illustrated here by analyzing PM emitted in two engine  
459 operation regimes. The fine statistical analysis of the CS action on size-selected  
460 particles revealed (despite the high removal efficiency) the “memory” of the  
461 initial (unstripped) composition of the particles, which was not possible with  
462 the polydisperse PM. This further stresses how important it is to sample and  
463 characterize size-selected particulate matter, especially since the chemical com-  
464 position of the smallest particles (with low contribution to the total mass in a  
465 polydisperse sample) cannot be otherwise inferred. Deposition on filters/sub-  
466 strates and offline analysis seems to be the only option here, as aerosol mass  
467 spectrometers are typically limited to sizes above  $\sim 50$  nm.

468 This work also showed that the smallest particles (10–32 nm) are the most af-  
469 fected by the CS, indicating that particles in this size range carry a larger volatile  
470 fraction. This conclusion concurs with the results of online aerodynamic-mass-  
471 mobility tandem measurements [40] performed in parallel with the collection of  
472 samples described here: on-line (physical) and off-line (chemical) investigations  
473 are in excellent agreement. The online measurements revealed an increasing  
474 contribution of the particle-bound volatile mass fraction toward smaller parti-  
475 cles sizes, as illustrated in Figure S8. The excellent agreement between these  
476 two completely independent (chemical and physical) characterization methods  
477 demonstrates the reliability of the used experimental approaches and validates  
478 the main conclusions of the study, which is also supported by theoretical in-  
479 vestigations [39] conducted in the PEMS4Nano project and showing the same  
480 trend of the SOF with size. Moreover, the obtained trend also matches previous

dynamometer and on-road testing showing that semi-volatile particles represent a significant fraction of the smallest nanoparticles [56, 57].

We demonstrated that a fine molecular-level characterization of the exhaust PM is necessary to precisely evaluate the effect of a CS, especially for the smallest ultra-fine particles. As the particles' outer organic layer consists of a multitude of chemical species (*e.g.* PAHs) and that the smallest particles tend to exhibit a larger volatile fraction, the ultra-fine PM could present a double risk – due to their small size they penetrate deeper in the respiratory system while also carrying a larger amount of potentially toxic compounds. This not only shows how important is the addition of oxidation catalysts in after-treatment systems of modern vehicles to remove the (potentially toxic) organic fraction from the engine exhaust, but also how crucial is the regulation of the small sub-23 nm particles.

## Acknowledgments

This study has received funding as a part of the PEMS4Nano project from the European Union's Horizon 2020 research and innovation programme under Grant Agreement No. 724145. Additionally, this work was supported by the French National Research Agency (ANR) under contract ANR-18-CE22-0019 (UNREAL) and through the PIA (Programme d'Investissement d'Avenir) under contract ANR-10-LABX-005 (LABEX CaPPA - Chemical and Physical Properties of the Atmosphere) and by the UK EPSRC Centre for Sustainable Road Freight (EP/R035199/1) and NERC Integrated Research Observation System for Clean Air (NE/T001909/1).

## References

- [1] C. Guerreiro, A. Ortiz, F. de Leeuw, M. Viana, Air quality 2018 - EEA report 12 2018, Publications Office of the European Union, 2018. doi: 10.2800/777411.
- [2] F. Karagulian, C. A. Belis, C. F. C. Dora, A. M. Prüss-Ustün, S. Bonjour, H. Adair-Rohani, M. Amann, Contributions to cities' ambient particulate matter (pm): A systematic review of local source contributions

- at global level, *Atmospheric Environment* 120 (2015) 475–483. doi:  
10.1016/j.atmosenv.2015.08.087.
- [3] J. H. Johnson, S. T. Bagley, L. D. Gradz, D. G. Leddy, A review of diesel  
particulate control technology and emissions effects, Horning Memorial  
Award Lecture SAE paper 940233 (1994). doi:10.4271/940233.
- [4] B. R. Stanmore, J. F. Brilhac, P. Gilot, The oxidation of soot: a review of  
experiments, mechanisms and models, *Carbon* 39 (2001) 2247–2268. doi:  
10.1016/S0008-6223(01)00109-9.
- [5] Z. D. Ristovski, B. Miljevic, N. C. Surawski, L. Morawska, K. M. Fong,  
F. Goh, I. A. Yang, Respiratory health effects of diesel particulate matter,  
*Respirology* 17 (2012) 201–212. doi:10.1111/j.1440-1843.2011.02109.  
x.
- [6] H.-S. Kwon, M. H. Ryu, C. Carlsten, Ultrafine particles: unique physico-  
chemical properties relevant to health and disease, *Experimental & Molec-  
ular Medicine* 52 (2020) 318–328. doi:10.1038/s12276-020-0405-1.
- [7] Y. Li, K. J. Lane, L. Corlin, A. P. Patton, J. L. Durant, M. Thanikachalam,  
M. Woodin, M. Wang, D. Brugge, Association of long-term near-highway  
exposure to ultrafine particles with cardiovascular diseases, diabetes and  
hypertension, *International journal of environmental research and public  
health* 14 (2017) 461–477. doi:10.3390/ijerph14050461.
- [8] B. A. Maher, I. A. Ahmed, V. Karloukovski, D. A. MacLaren, P. G. Foulds,  
D. Allsop, D. M. Mann, R. Torres-Jardón, L. Calderon-Garciduenas, Mag-  
netite pollution nanoparticles in the human brain, *Proceedings of the Na-  
tional Academy of Sciences* 113 (2016) 10797–10801. doi:10.1073/pnas.  
1605941113.
- [9] N. D. Saenen, H. Bové, C. Steuwe, M. B. Roeffaers, E. B. Provost,  
W. Lefebvre, C. Vanpoucke, M. Ameloot, T. S. Nawrot, Children’s uri-  
nary environmental carbon load. a novel marker reflecting residential am-  
bient air pollution exposure?, *American Journal of Respiratory and Critical  
Care Medicine* 196 (2017) 873–881. doi:10.1164/rccm.201704-07970C.

- 541 [10] H. Bové, E. Bongaerts, E. Slenders, E. M. Bijnens, N. D. Saenen, W. Gyselaers, P. Van Eyken, M. Plusquin, M. B. Roeffaers, M. Ameloot, et al.,  
542 Ambient black carbon particles reach the fetal side of human placenta, *Nature communications* 10 (2019) 3866. doi:10.1038/s41467-019-11654-3.  
543  
544
- 545 [11] L. Setti, F. Passarini, G. De Gennaro, P. Barbieri, A. Pallavicini, M. Ruscio, P. Piscitelli, A. Colao, A. Miani, Searching for SARS-COV-2 on particulate  
546 matter: A possible early indicator of COVID-19 epidemic recurrence, *International Journal of Environmental Research and Public Health* 17 (2020)  
547 2986–2991. doi:10.3390/ijerph17092986.  
548  
549
- 550 [12] D. Contini, F. Costabile, Does air pollution influence COVID-19 outbreaks?, *Atmosphere* 11 (2020) 377–382. doi:10.3390/atmos11040377.  
551
- 552 [13] H. C. Frey, Trends in onroad transportation energy and emissions, *Journal of the Air and Waste Management Association* 68 (2018) 514–563. doi:  
553 10.1080/10962247.2018.1454357.  
554
- 555 [14] P. Bielaczyc, J. Woodburn, Trends in automotive emission legislation: impact on ld engine development, fuels, lubricants and test methods: a global  
556 view, with a focus on wltc and rde regulations, *Emission Control Science and Technology* 5 (2019) 86–98. doi:10.1007/s40825-019-0112-3.  
557  
558
- 559 [15] B. Giechaskiel, A. Joshi, L. Ntziachristos, P. Dilara, European regulatory framework and particulate matter emissions of gasoline light-duty vehicles:  
560 A review, *Catalysts* 9 (2019) 586. doi:10.3390/catal9070586.  
561
- 562 [16] G. C. Koltsakis, A. M. Stamatelos, Catalytic automotive exhaust aftertreatment, *Progress in Energy and Combustion Science* 23 (1997) 1–39.  
563 doi:10.1016/S0360-1285(97)00003-8.  
564
- 565 [17] E. Meloni, V. Palma, Most recent advances in diesel engine catalytic soot abatement: Structured catalysts and alternative approaches, *Catalysts* 10  
566 (2020) 745. doi:10.3390/catal10070745.  
567
- 568 [18] A. Mamakos, M. Schwelberger, M. Fierz, B. Giechaskiel, Effect of selective catalytic reduction on exhaust nonvolatile particle emissions of euro vi  
569

- heavy-duty compression ignition vehicles, *Aerosol Science and Technology* 53 (2019) 898–910. doi:10.1080/02786826.2019.1610153.
- [19] P. Karjalainen, L. Pirjola, J. Heikkilä, T. Lähde, T. Tzamkiozis, L. Ntziachristos, J. Keskinen, T. Rönkkö, Exhaust particles of modern gasoline vehicles: A laboratory and an on-road study, *Atmospheric Environment* 97 (2014) 262–270. doi:10.1016/j.atmosenv.2014.08.025.
- [20] M. Williams, R. Minjares, A technical summary of euro 6/vi vehicle emission standards. icct (international council on clean transportation) briefing (2016).  
URL <https://theicct.org/publications/technical-summary-euro-6vi-vehicle-emissionstandards>
- [21] B. Giechaskiel, U. Manfredi, G. Martini, Engine exhaust solid sub-23 nm particles: I. literature survey, *SAE International Journal of Fuels and Lubricants* 7 (2014) 950–964. doi:10.4271/2014-01-2834.
- [22] B. Giechaskiel, J. Vanhanen, M. Vakeva, G. Martini, Investigation of vehicle exhaust sub-23 nm particle emissions, *Aerosol Science and Technology* 51 (2017) 626–641. doi:10.4271/2014-01-2834.
- [23] G. Martini, T. Grigoratos, PMP IWG Progress Report; 81st UNECE GRPE session, 9–11 June 2020 (2020).  
URL <http://www.unece.org/fileadmin/DAM/trans/doc/2020/wp29grpe/GRPE-81-31e.pdf>
- [24] B. Giechaskiel, E. Schiefer, W. Schindler, H. Axmann, C. Dardiotis, Overview of soot emission measurements instrumentation: From smoke and filter mass to particle number, *SAE International Journal of Engines* 6 (2013) 10–22. doi:10.4271/2013-01-0138.
- [25] PEMs4Nano. European Union’s Horizon 2020 research and innovation programme under grant agreement Nr. 724145, accessed on 17 August 2020 (2020).  
URL <https://pems4nano.eu>

- 599 [26] DownToTen. European Union’s Horizon 2020 research and innovation  
600 programme under grant agreement Nr. 724085, accessed on 17 August 2020  
601 (2020).  
602 URL <https://downtoten.com>
- 603 [27] SUREAL-23. European Union’s Horizon 2020 research and innovation  
604 programme under grant agreement Nr. 724136, accessed on 17 August 2020  
605 (2020).  
606 URL <http://soreal-23.cperi.certh.gr>
- 607 [28] B. Giechaskiel, A. Mamakos, J. Woodburn, A. Szczotka, P. Bielaczyc, Eval-  
608 uation of a 10 nm particle number portable emissions measurement system  
609 (PEMS), *Sensors* 19 (2019) 5531. doi:10.3390/s19245531.
- 610 [29] B. Giechaskiel, P. Bonnel, A. Perujo, P. Dilara, Solid particle number (SPN)  
611 portable emissions measurement systems (PEMS) in the European legis-  
612 lation: A review, *International Journal of Environmental Research and*  
613 *Public Health* 16 (2019) 4819. doi:10.3390/ijerph16234819.
- 614 [30] B. Giechaskiel, T. Lähde, S. Gandi, S. Keller, P. Kreutziger, A. Ma-  
615 makos, Assessment of 10-nm Particle Number (PN) Portable Emissions  
616 Measurement Systems (PEMS) for Future Regulations, *International Jour-*  
617 *nal of Environmental Research and Public Health* 17 (2020) 3878. doi:  
618 10.3390/ijerph17113878.
- 619 [31] B. Giechaskiel, A. D. Melas, T. Lähde, G. Martini, Non-Volatile Parti-  
620 cle Number Emission Measurements with Catalytic Strippers: A Review,  
621 *Vehicles* 2 (2020) 342–364. doi:10.3390/vehicles2020019.
- 622 [32] B. Giechaskiel, Y. Drossinos, Theoretical investigation of volatile removal  
623 efficiency of particle number measurement systems, *SAE International*  
624 *Journal of Engines* 3 (2010) 1140–1151. doi:10.4271/2010-01-1304.
- 625 [33] H. Yamada, K. Funato, H. Sakurai, Application of the PMP methodology  
626 to the measurement of sub-23 nm solid particles: calibration procedures, ex-  
627 perimental uncertainties, and data correction methods, *Journal of Aerosol*  
628 *Science* 88 (2015) 58–71. doi:10.1016/j.jaerosci.2015.06.002.

- [34] A. Melas, V. Koidi, D. Deloglou, E. Daskalos, D. Zarvalis, E. Papaioannou, A. Konstandopoulos, Development and evaluation of a catalytic stripper for the measurement of solid ultrafine particle emissions from internal combustion engines, *Aerosol Science and Technology* 54 (2020) 704–717. doi:10.1080/02786826.2020.1718061.
- [35] S. Amanatidis, L. Ntziachristos, B. Giechaskiel, D. Katsaounis, Z. Samaras, A. Bergmann, Evaluation of an oxidation catalyst (“catalytic stripper”) in eliminating volatile material from combustion aerosol, *Journal of aerosol science* 57 (2013) 144–155. doi:10.1016/j.jaerosci.2012.12.001.
- [36] L. Ntziachristos, S. Amanatidis, Z. Samaras, B. Giechaskiel, A. Bergmann, Use of a catalytic stripper as an alternative to the original PMP measurement protocol, *SAE International Journal of Fuels and Lubricants* 6 (2013) 532–541. doi:10.4271/2013-01-1563.
- [37] S. Amanatidis, L. Ntziachristos, P. Karjalainen, E. Saukko, P. Simonen, N. Kuittinen, P. Aakko-Saksa, H. Timonen, T. Rönkkö, J. Keskinen, Comparative performance of a thermal denuder and a catalytic stripper in sampling laboratory and marine exhaust aerosols, *Aerosol Science and Technology* 52 (2018) 420–432. doi:10.1080/02786826.2017.1422236.
- [38] C. Focsa, D. Duca, J. A. Noble, M. Vojkovic, Y. Carpentier, C. Pirim, C. Betrancourt, P. Desgroux, T. Trischer, J. Spielvogel, M. Rahman, A. Boies, K. F. Lee, A. N. Bhave, S. Legendre, O. Lancry, P. Kreutziger, M. Rieker, Multi-technique physico-chemical characterization of particles generated by a gasoline engine: towards measuring tailpipe emissions below 23 nm, *Atmospheric Environment* 235 (2020) 117642. doi:10.1016/j.atmosenv.2020.117642.
- [39] K. F. K. Lee, N. Eaves, S. Mosbach, D. Ooi, J. Lai, A. Bhave, A. Manz, J. N. J. Geiler, J. A. J. Noble, D. Duca, C. Focsa, J. Niklas, G. Robert, B. Gmbh, J. A. J. Noble, D. Duca, Model Guided Application for Investigating Particle Number (PN) Emissions in GDI Spark Ignition Engines, *SAE International Journal of Advances and Current Practices in Mobility-V128-99EJ* 26 (2019) 76–88. doi:10.4271/2019-26-0062.

- [40] M. Kazemimanesh, M. Rahman, D. Duca, T. Johnson, A. Addad, G. Giannopoulos, C. Focsa, A. Boies, Morphology and volatility of particulate emissions from gasoline direct injection engine using aerodynamic diameter, mobility diameter, and mass measurements in tandem, submitted to Aerosol Science and Technology (2020).
- [41] L. D. Ngo, D. Duca, J. A. Noble, A. R. Ikhenazene, M. Vojkovic, Y. Carpentier, C. Irimiea, Chemical discrimination of the particulate and gas phases of miniCAST exhausts using a two-filter collection method, Atmospheric Measurement Techniques 13 (2020) 951–967. doi:10.5194/amt-13-951-2020.
- [42] A. Faccinetto, P. Desgroux, M. Ziskind, E. Therssen, C. Focsa, High-sensitivity detection of polycyclic aromatic hydrocarbons adsorbed onto soot particles using laser desorption/laser ionization/time-of-flight mass spectrometry: An approach to studying the soot inception process in low-pressure flames, Combustion and Flame 158 (2011) 227–239. doi:10.1016/j.combustflame.2010.08.012.
- [43] A. Faccinetto, C. Focsa, P. Desgroux, M. Ziskind, Progress toward the Quantitative Analysis of PAHs Adsorbed on Soot by Laser Desorption/Laser Ionization/Time-of-Flight Mass Spectrometry, Environmental Science and Technology 49 (2015) 10510–10520. doi:10.1021/acs.est.5b02703.
- [44] C. Irimiea, A. Faccinetto, Y. Carpentier, I. K. Ortega, N. Nuns, E. Therssen, P. Desgroux, C. Focsa, A comprehensive protocol for chemical analysis of flame combustion emissions by secondary ion mass spectrometry, Rapid Communications in Mass Spectrometry 32 (2018) 1015–1025. doi:10.1002/rcm.8133.
- [45] C. Irimiea, A. Faccinetto, X. Mercier, I.-K. Ortega, N. Nuns, E. Therssen, P. Desgroux, C. Focsa, Unveiling trends in soot nucleation and growth: When secondary ion mass spectrometry meets statistical analysis, Carbon 144 (2019) 815–830. doi:10.1016/j.carbon.2018.12.015.
- [46] D. Duca, C. Irimiea, A. Faccinetto, J. A. Noble, M. Vojkovic, Y. Carpentier,

- 691 I. K. Ortega, C. Pirim, C. Focsa, On the benefits of using multivariate  
692 analysis in mass spectrometric studies of combustion-generated aerosols,  
693 Faraday Discussions 218 (2019) 115–137. doi:10.1039/C8FD00238J.
- 694 [47] T. Adam, R. R. Baker, R. Zimmermann, Characterization of puff-by-puff  
695 resolved cigarette mainstream smoke by single photon ionization-time-of-  
696 flight mass spectrometry and principal component analysis, Journal of  
697 Agricultural and Food Chemistry 55 (2007) 2055–2061. doi:10.1021/  
698 jf062360x.
- 699 [48] W. Li, Volcano plots in analyzing differential expressions with mRNA mi-  
700 croarrays, Journal of Bioinformatics and Computational Biology 10 (2012)  
701 1231003. doi:10.1142/S0219720012310038.
- 702 [49] L. Shi, W. Tong, H. Fang, U. Scherf, J. Han, R. K. Puri, F. W. Frueh, F. M.  
703 Goodsaid, L. Guo, Z. Su, T. Han, J. C. Fuscoe, Z. A. Xu, T. A. Patterson,  
704 H. Hong, Q. Xie, R. G. Perkins, J. J. Chen, D. A. Casciano, Cross-platform  
705 comparability of microarray technology: Intra-platform consistency and  
706 appropriate data analysis procedures are essential, BMC Bioinformatics 6  
707 (2005) S12–S26. doi:10.1186/1471-2105-6-S2-S12.
- 708 [50] D. Delhay, F. X. Ouf, D. Ferry, I. K. Ortega, O. Penanhoat, S. Peillon,  
709 F. Salm, X. Vancassel, C. Focsa, C. Irimiea, N. Harivel, B. Perez, E. Quin-  
710 ton, J. Yon, D. Gaffie, The MERMOSE project: Characterization of partic-  
711 ulate matter emissions of a commercial aircraft engine, Journal of Aerosol  
712 Science 105 (2017) 48–63. doi:10.1016/j.jaerosci.2016.11.018.
- 713 [51] M. A. Bari, G. Baumbach, B. Kuch, G. Scheffknecht, Particle-phase con-  
714 centrations of polycyclic aromatic hydrocarbons in ambient air of rural res-  
715 idential areas in southern Germany, Air Quality, Atmosphere and Health 3  
716 (2010) 103–116. doi:10.1007/s11869-009-0057-8.
- 717 [52] T. Ferge, E. Karg, A. Schröppel, K. R. Coffee, H. J. Tobias, M. Frank, E. E.  
718 Gard, R. Zimmermann, Fast determination of the relative elemental and  
719 organic carbon content of aerosol samples by on-line single-particle aerosol  
720 time-of-flight mass spectrometry, Environmental Science and Technology  
721 40 (10) (2006) 3327–3335. doi:10.1021/es050799k.

- 722 [53] J. Pagels, D. D. Dutcher, M. R. Stolzenburg, P. H. McMurry, M. E. Gälli,  
723 D. S. Gross, Fine-particle emissions from solid biofuel combustion stud-  
724 ied with single-particle mass spectrometry: Identification of markers for  
725 organics, soot, and ash components, *Journal of Geophysical Research At-*  
726 *mospheres* 118 (2013) 859–870. doi:10.1029/2012JD018389.
- 727 [54] O. B. Popovicheva, C. Irimiea, Y. Carpentier, I. K. Ortega, E. D. Kireeva,  
728 N. K. Shonija, J. Schwarz, M. Vojtíšek-Lom, C. Focsa, Chemical composi-  
729 tion of diesel/biodiesel particulate exhaust by FTIR spectroscopy and mass  
730 spectrometry: Impact of fuel and driving cycle, *Aerosol and Air Quality*  
731 *Research* 17 (2017) 1717–1734. doi:10.4209/aaqr.2017.04.0127.
- 732 [55] S. E. Stein, A. Fahr, High-temperature stabilities of hydrocarbons, *Journal*  
733 *of Physical Chemistry* 89 (1985) 3714–3725. doi:10.1021/j100263a027.
- 734 [56] J. Ko, K. Kim, W. Chung, C. L. Myung, S. Park, Characteristics of on-  
735 road particle number (PN) emissions from a GDI vehicle depending on a  
736 catalytic stripper (CS) and a metal-foam gasoline particulate filter (GPF),  
737 *Fuel* 238 (2019) 363–374. doi:10.1016/j.fuel.2018.10.091.
- 738 [57] A. Momenimovahed, D. Handford, M. D. Checkel, J. S. Olfert, Particle  
739 number emission factors and volatile fraction of particles emitted from on-  
740 road gasoline direct injection passenger vehicles, *Atmospheric Environment*  
741 102 (2015) 105–111. doi:10.1016/j.atmosenv.2014.11.045.